Electronic Supplementary Information

Enhanced water stability and high CO_2 storage capacity of a Lewis basic sites-containing zirconium metal-organic framework

Selçuk Demir,[a,*] Nuray Bilgin,[a] Hamide Merve Cepni,[a] Hiroyasu Furukawa,[b] Fatih Yilmaz,[a] Cigdem Altintas,[c] and Seda Keskin[c]

[a] Recep Tayyip Erdoğan University, Faculty of Arts and Sciences, Department of Chemistry, 53100, Rize, Turkey.

[b] Department of Chemistry, University of California-Berkeley, Berkeley, CA 94720, USA.

[c] Department of Chemical and Biological Engineering, Koc University, Istanbul, Turkey.

*To whom correspondence should be addressed. Email: selcuk.demir@erdogan.edu.tr

Table of Contents

1. Experimental details for linker synthesis

Synthesis of 6,6′-dimethyl-2,2′-bipyridine-5,5′-dicarboxylic acid, (Me_2bipyH_2)

Ethyl 2-methylnicotinate (ethyl 2-methylpyridine-3-carboxylate) (4.0 g, 23 mmol) refluxed under nitrogen atmosphere at 180 °C for six days employing 5% Pd/C (0.1 g) as a catalyst with a magnetic stirrer. The formed colorless crystals dissolved in acetone and separated from Pd/C. The solution was evaporated under vacuum and corresponding product, diethyl 6,6′-dimethyl-[2,2′-bipyridine]-5,5′-dicarboxylate obtained. The obtained ester (0.090 g, 0.27 mmol) hydrolyzed in acetone-ethanol-water (1.5:1:1 *v*/*v*, 35 mL) containing NaOH (0.05 g) for 24 hours at room temperature. After the evaporation of ethanol and acetone, the solution was acidified by HCl until pH = 3. The formed H_2Me_2Bipy was purified using preparative thin layer chromatography plates. Yield is 25% based on ethyl 2-methylnicotinate. The reaction scheme and IR and NMR spectra were shown in Scheme S1 and Figs. S1-S2, respectively.

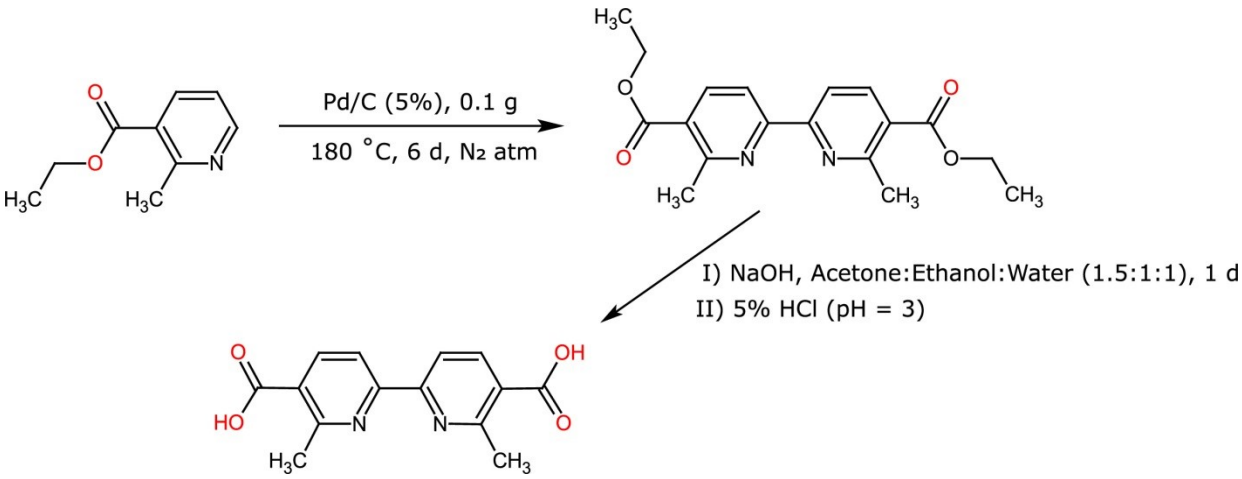

Scheme S1. Reaction scheme of H_2Me_2Bipy.

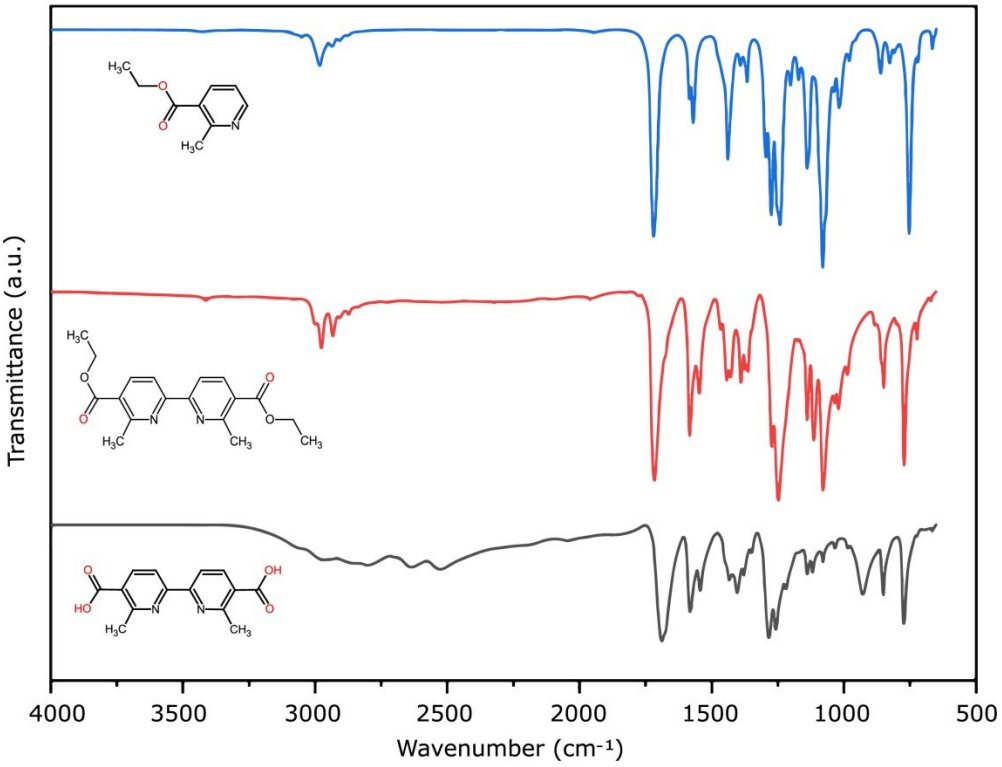

Fig. S1 FTIR spectra of ethyl 2-methylnicotinate, di-ester, and H_2Me_2Bipy.

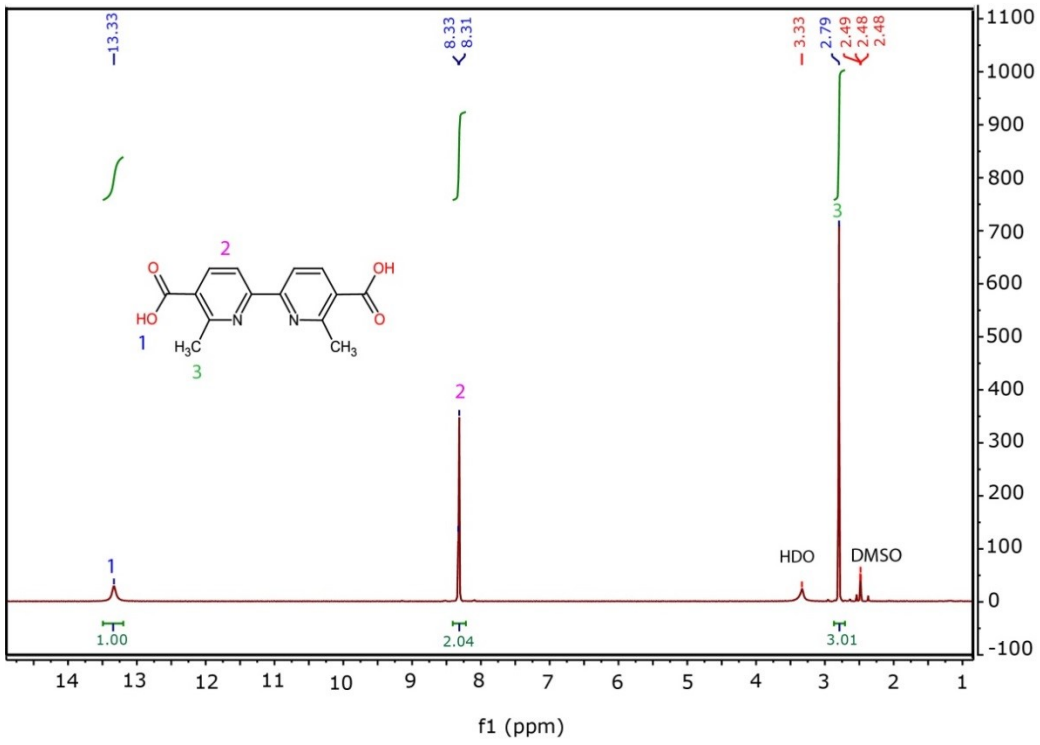

Fig. S2 ^1H NMR spectrum of H_2Me_2Bipy.

2. Characterization of MOFs

Selected IR data for the compounds are summarized in Table S1. The IR spectra of the MOFs showed expected vibrations (Fig. S3). A broad band at *ca.* 3400 cm^{-1} in the spectra of the MOFs is assigned to ν(OH) vibration of the unavoidable water molecules. The compounds exhibit two very strong bands at 1585 cm^{-1} and 1400 cm^{-1} region attributable to the $\nu_{asym}(COO^{-})$ and $\nu_{sym}(COO^{-})$.

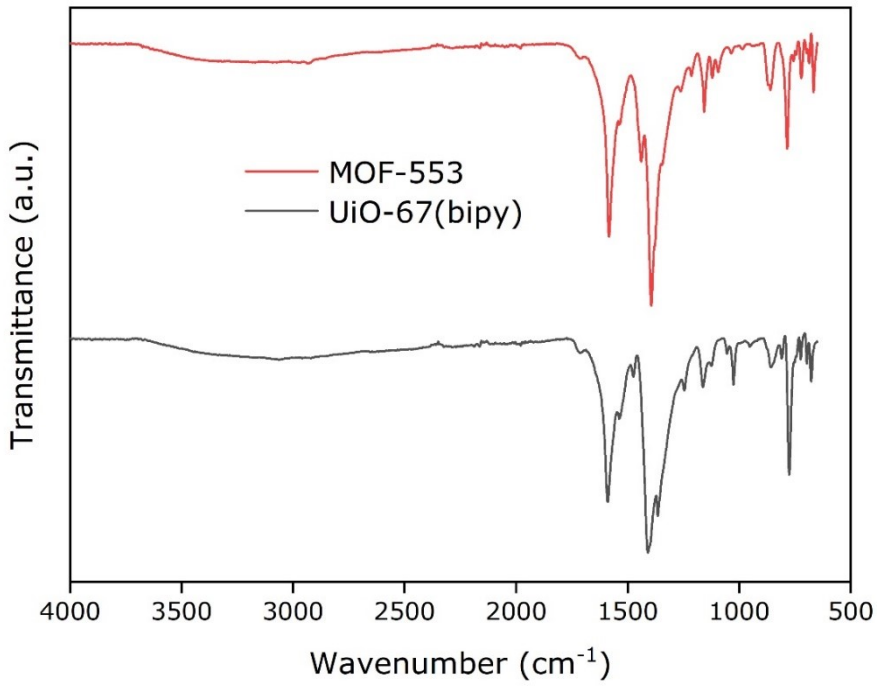

Fig. S3 FTIR spectra of MOF-553 and UiO-67(bipy).

Table S1 IR spectral data for MOFs and linker

Compounds	ν (CH)	ν(C=O)	$\nu_{asym}(COO^{-})$	$\nu_{sym}(COO^{-})$
H_2Me_2Bipy	3075, 2900	1693 (COOH)	-	-
UiO-67(bipy)	3061	-	1589 vs	1409 vs
MOF-553	3061, 2935	-	1583 vs	1394 vs

For the determination of unit cell dimensions, a microcrystalline sample of MOF-553 was gently ground and placed on a sample holder equipped with a zero-background Si plate. Powder X-ray diffraction (PXRD) data were collected during an overnight scan in the 2θ range of 4–70° with 0.013° steps using a Malvern Panalytical Empyrean diffractometer equipped with Cu - K_α radiation (λ = 1.5418 Å), a PIXcel1D detector with Medipix3, and mounting the following optics: Göbel mirror, fixed divergence slit (0.5 mm), receiving slit (3 mm), and secondary beam Soller slits (2.29°). The generator was set at 45 kV and 40 mA.

A standard peak search, followed by indexing via the single value decomposition approach,[1] as implemented in TOPAS-Academic,[2] allowed the determination of approximate unit cell dimensions. Precise unit cell dimensions were determined by performing a structureless Le Bail refinement in TOPAS-Academic.

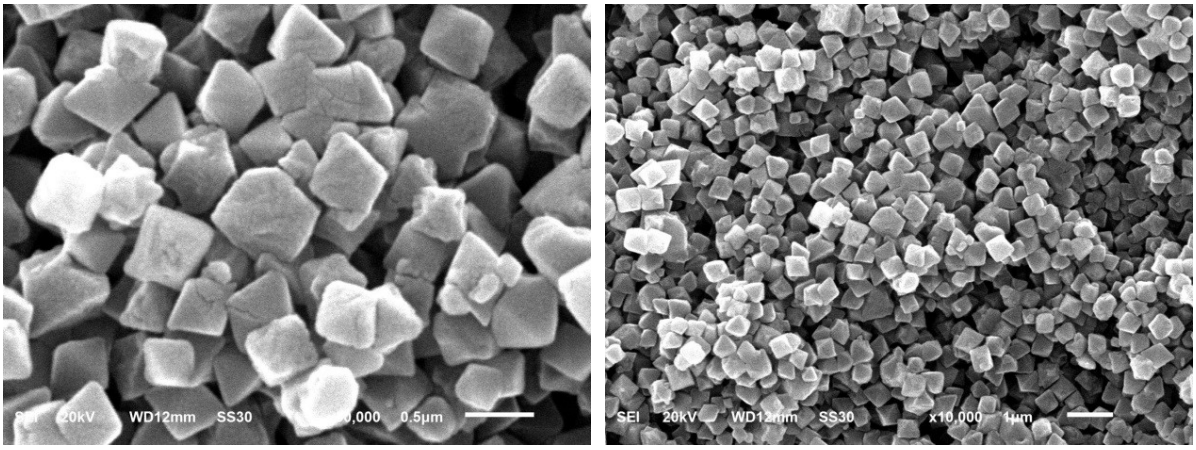

Fig. S4 SEM images of MOF-553.

To evaluate the absence of the occluded molecules in the pores and thermal stability of MOF-553 and UiO-67(bipy), thermogravimetric analysis (TGA) measurement was performed under a dynamic air atmosphere. Weight losses at 25–120 °C are attributed to occluded water molecules (physisorbed water) within the pores, which is unavoidable for most MOFs. In contrast, the drastic weight loss was observed after 400 °C. Therefore, it can be concluded that the prepared materials are well activated and stable up to 400 °C.

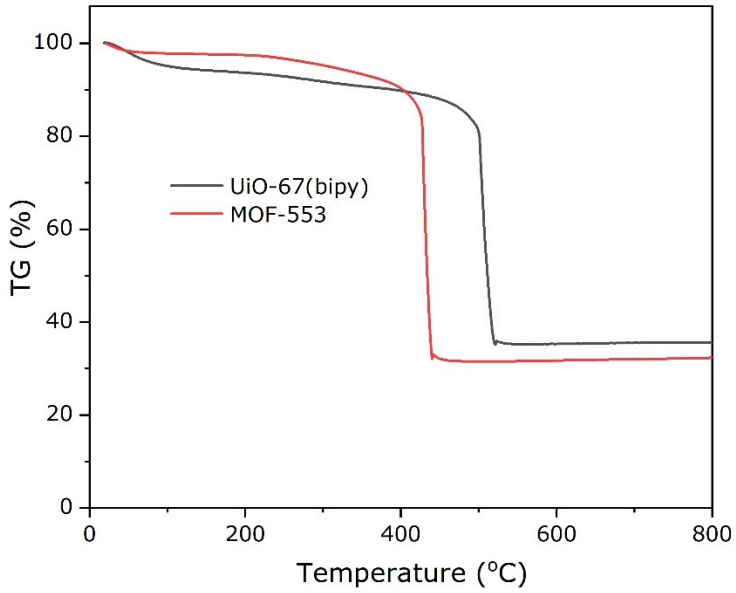

Fig. S5 TGA curves of MOF-553 and UiO-67(bipy).

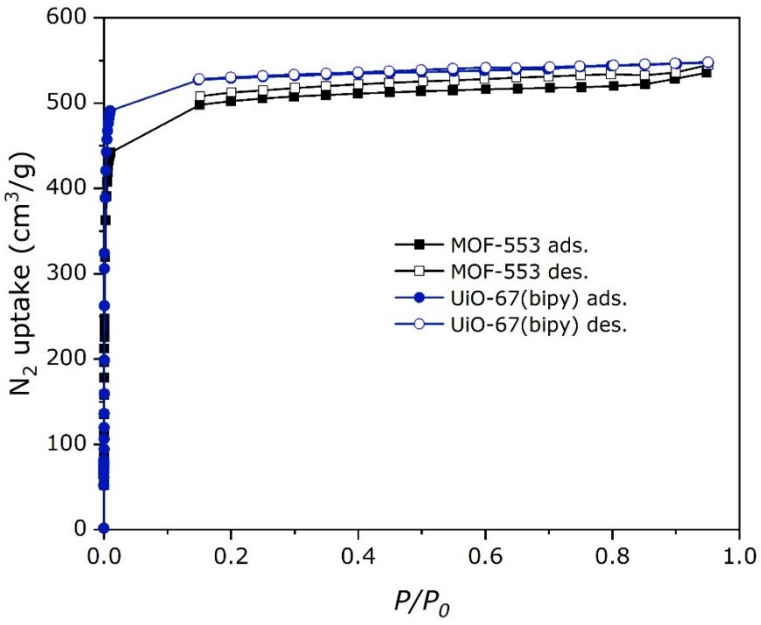

Fig. S6 N_2 isotherms of MOF-553 and UiO-67(bipy) measured at 77 K.

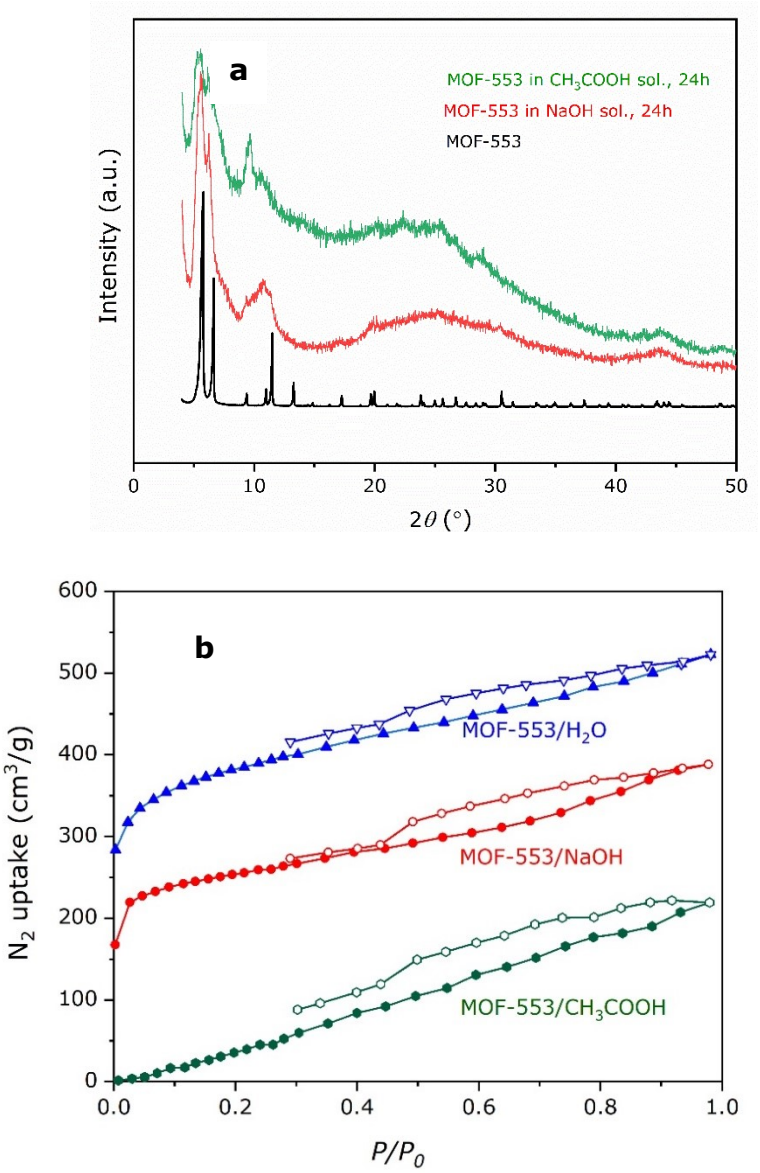

Fig. S7 a) PXRD patterns for MOF-553 (black), MOF-553 treated in CH_3COOH (green) and in NaOH solution (red); **b**) Adsorption-desorption isotherms of MOF-553/H_2O, MOF-553/NaOH, and MOF-553/CH_3COOH (adsorption: filled circles, desorption: empty circles)

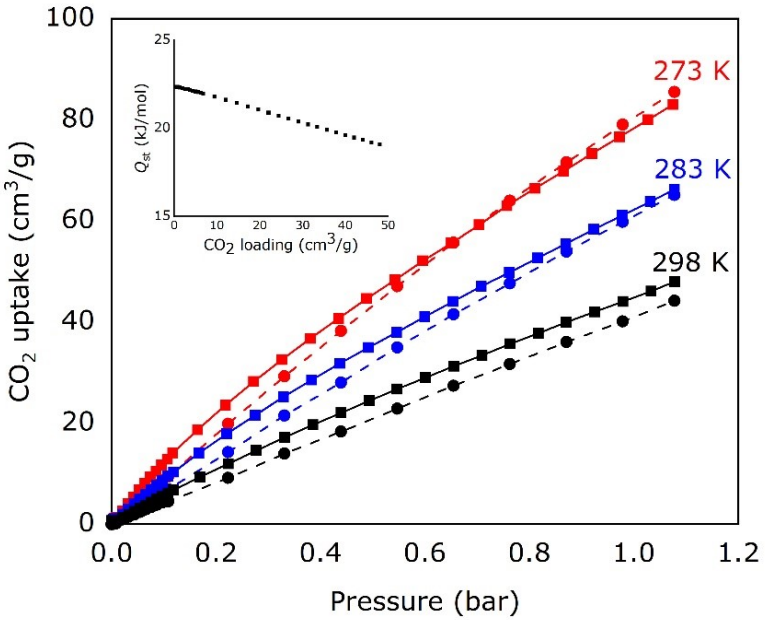

Fig. S8 CO_2 adsorption isotherms and Q_{st} graph (inset) of MOF-553. Squares show the experimental data and circles represent the simulation results.

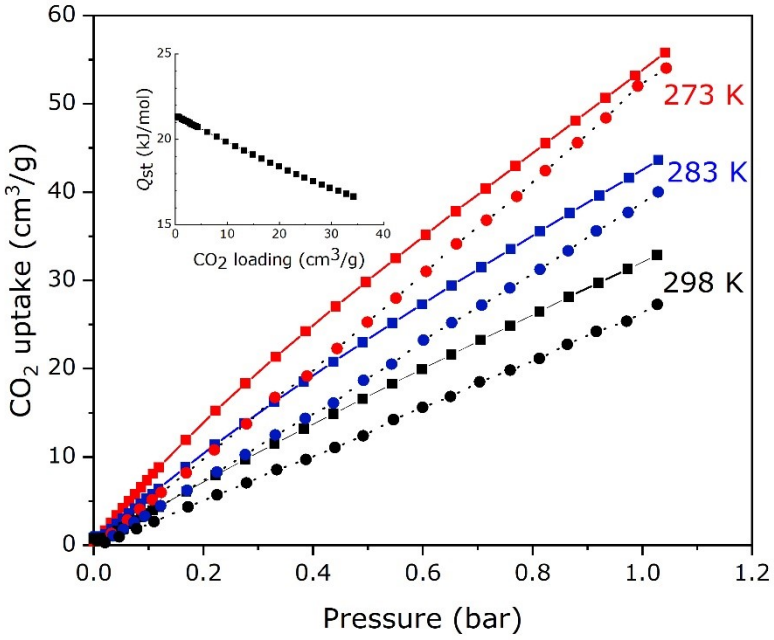

Fig. S9 CO_2 adsorption isotherms and *Q*st curve (inset) of UiO-67(bipy). Squares show the experimental data and circles represent the simulation results.

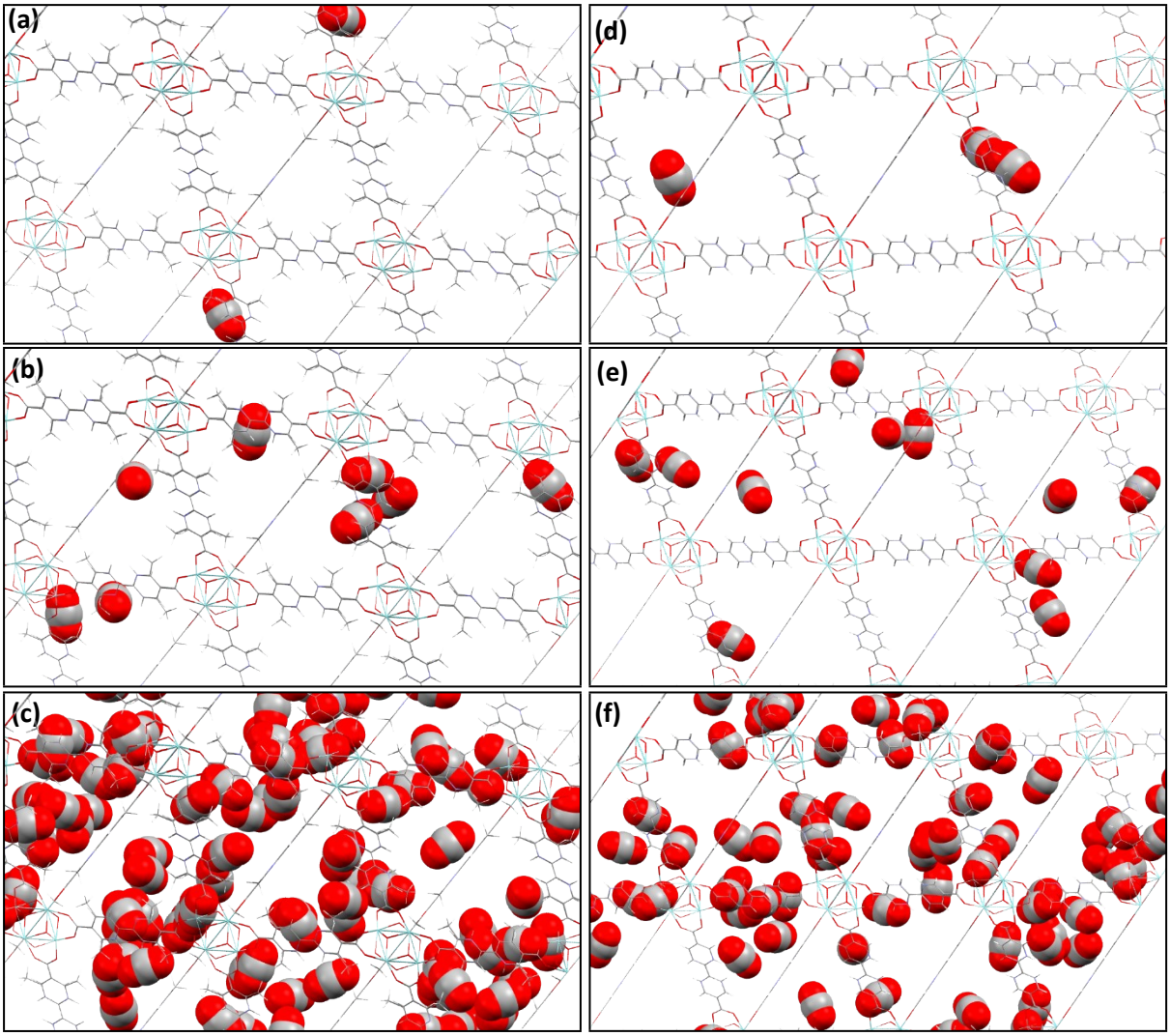

Fig. S10 Zoom-in view of CO_2 adsorption sites obtained from GCMC simulations at 0.01, 0.1, and 1 bar for (a-c) MOF-553, (d-f) UiO-67(bipy).

3. Setup for humid gas stream

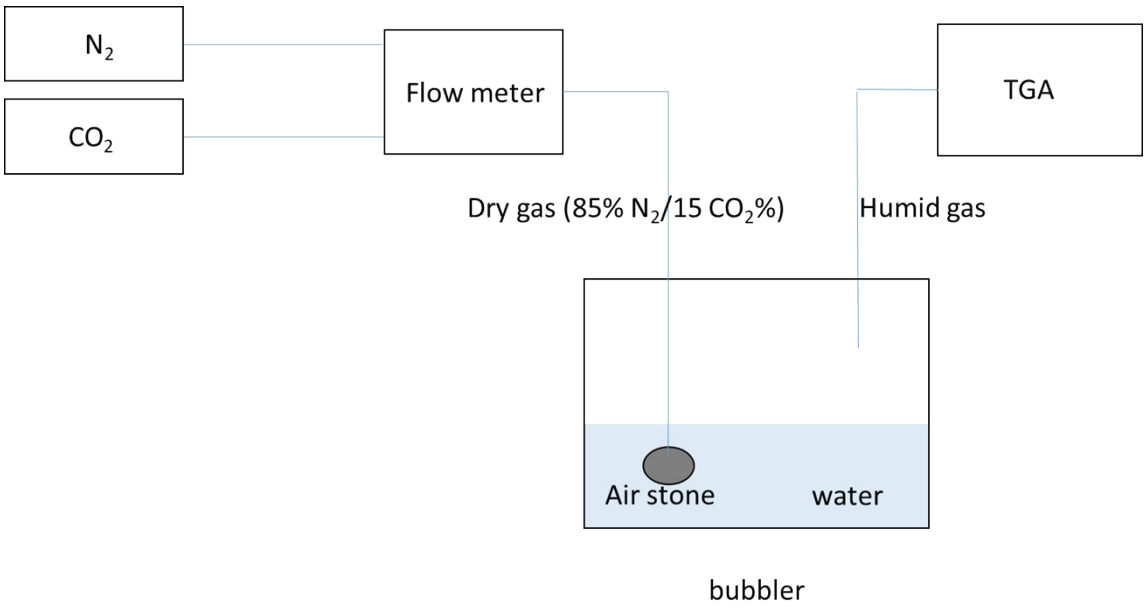

Fig. S11 Set up for preparation of humid gas stream (N_2/CO_2 = 85/15).

TGA results of dry N_2 (pure N_2), humid N_2, dry CO_2 (pure CO_2) and humid CO_2 adsorption experiments on MOF-553 with or without water were shown in Fig. S12. Consistent with TGA, under dry N_2 atmosphere the weight increase is rather small than pure and humid CO_2 conditions. Thus we can conclude that MOF-553 adsorbs a small amount of N_2 and H_2O+N_2 at experimental conditions. Thus, it may be acceptable to neglect N_2 co-adsorption in these multicomponent measurements. Under humid CO_2 stream the mass of MOF-553 is increased (3.5%) relative to the dry CO_2 (2.0%). Therefore, the weight difference between the dry and humid CO_2 experiments should primarily be due to water adsorption. The water content is estimated to be 1.5% at 38 °C by comparison of dry and humid CO_2 gas results on TGA, and it is comparable with the results of Long *et al.*[3] which reported as 1.3%. Please note that Fig. S12 is recorded under binary gas mixtures and Fig. 6 is recorded under flue gas conditions and the uptake amount subject to change as verified via simulations.

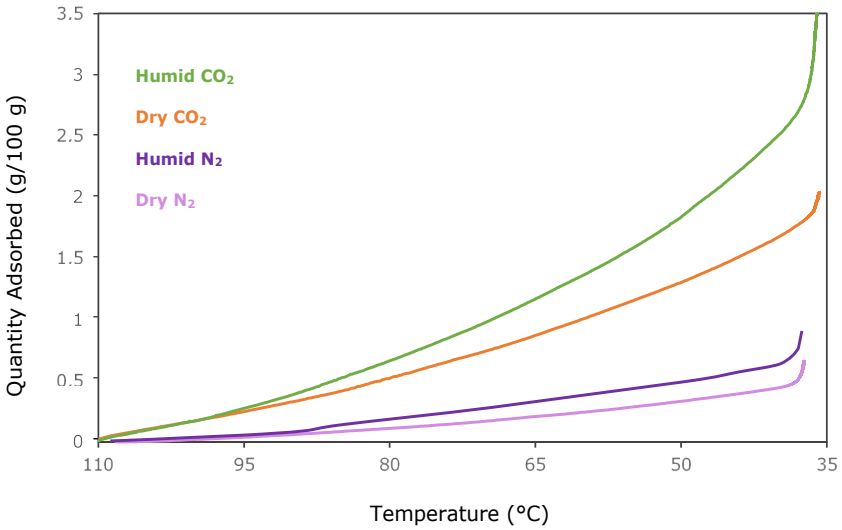

Fig. S12 TGA results of pure and binary gas uptake obtained employing the prepared set up (Fig. S11) (dry N_2: pure N_2; humid N_2: N_2+H_2O; dry CO_2: pure CO_2; humid CO_2: CO_2+H_2O).

References

1 A. Coelho, *J. Appl. Cryst.,* 2003, **36**, 86-95.
2 A. Coelho, TOPAS-Academic, Version 4.1, Coelho Software, Brisbane, 2007.
3 P.J. Milner, R.L. Siegelman, A.C. Forse, M.I. Gonzalez, T. Runčevski, J.D. Martell, J.A. Reimer, and J.R. Long, *J. Am. Chem. Soc.* 2017, **139**, 13541−13553.